PUBLICATIONS OF THE ASTRONOMICAL SOCIETY OF THE PACIFIC
97:877-884, October 1985

RADAR OBSERVATIONS OF ASTEROIDS AND COMETS*

STEVEN J. OSTRO
Jet Propulsion Laboratory, California Institute of Technology, 4800 Oak Grove Drive, Pasadena, California 91109

Radar observations of asteroids and comets provide information about these objects' sizes, shapes, spin vectors, decimeter-scale morphology, topographic relief, regolith porosity, and metal concentration. On average, small, near-earth asteroids are rougher at decimeter scales than comets or mainbelt asteroids. Asteroid 2 Pallas is smoother than the moon at decimeter scales but much rougher than the moon at some much larger scale(s). There is at least a five-fold variation in the radar albedos of main-belt asteroids, implying substantial variation in these objects' surface porosities or metal concentrations. The highest albedo estimate, for 16 Psyche, is consistent with a metal concentration near unity and lunar porosities. The radar polarization signature of the near-earth object 2101 Adonis is anomalous, resembling that of Jupiter's satellite Callisto more than that of any other radar-detected planetary target. The echo spectra of comet *IRAS*-Araki-Alcock reveal an irregular, ~ 7-km sized nucleus and an associated debris swarm, at least 10^3 times larger than the nucleus and comprised of particles at least a centimeter in size.

Key words: asteroids–comets–radar

I. Introduction

There are rare occasions in which astronomers can anticipate the initial close-up looks via spacecraft of entities studied previously only through telescopes. For scientists engaged in the study of the solar system's asteroids and comets, next year will be such a time. During 1986, we expect our first spacecraft flybys of two objects which represent extremes of the solar system's small-body population: a large main-belt asteroid, 29 Amphitrite, and the most famous short-period comet, Halley. These encounters comprise a critical first step toward detailed characterization of an enormous and extremely diverse assortment of solid planetary objects whose thorough exploration is prerequisite for an accurate understanding of the origin and evolution of our planetary system.

As we eagerly await the "Year of Halley and Amphitrite," it is appropriate to note certain distinguishing characteristics of asteroid/comet research. First, asteroids and comets are unique among large astronomical populations in that they can be satisfactorily characterized in the foreseeable future via the luxury of spacecraft investigation. (Of course, the prospect of imminent testability of empirical hypotheses is one of the distinct sources of pleasure and excitement in modern planetary science!) Second, since our goal in asteroid/comet studies is to understand enormous populations, the coupling between spacecraft and ground-based efforts is especially tight. Much of the scientific value of spacecraft missions will rest on our ability to extrapolate confidently from the mission targets to parent populations. Consequently, in contrast with the situation for the major planets and satellites, successful space missions to asteroids will enhance the value of existing ground-based data and will catalyze ground-based observing programs.

Current concepts of the nature of the asteroid/comet population rely most heavily on ground-based observations involving *UBV* photometry and polarimetry, spectrophotometry, IR radiometry, and light curves, in addition to search/discovery surveys. By comparison, radar and stellar-occultation timing have been applied to only a handful of small bodies. However, some of our most reliable inferences of small-body physical properties are for objects studied with one or both of these techniques.

Radar observations are powerful for several reasons. First, determination of the distribution of echo power in Doppler frequency and/or time delay can provide spatial resolution of an asteroid in a manner independent of the target's apparent angular extent. Second, radar wavelengths provide sensitivity to (1) surface and subsurface structure at scales orders of magnitude larger than those probed by optical methods but smaller than target dimensions, and (2) regolith porosity and metal concentration, two parameters which are poorly determined by VIS/IR methods. Furthermore, radar constraints on spin vector, size, and shape are distinct from, and complementary to, optical constraints on these quantities.

Efforts to use radar to study asteroids and comets expanded dramatically in 1980, and these objects now constitute 34 of the 43 radar-detected planetary targets (Table I). In this article, I will describe radar techniques, emphasizing the logical basis for inferring physical properties from radar measurements. I will review briefly the results to date, focusing on a few objects to convey some of the recent highlights of this research and to demonstrate the synergism between radar and other ground-based techniques. The recent results greatly enhance our knowledge of the small-body population and provide tantalizing hints of what next year's spacecraft flybys might reveal.

*An invited paper presented at the Symposium on New Directions in Asteroid and Comet Research at the 97th Annual Meeting of the Astronomical Society of the Pacific, Northern Arizona University, Flagstaff, June 1985.

TABLE I

RADAR-DETECTED ASTEROIDS AND COMETS

Mainbelt Asteroids (Ostro et al. 1985a)

1 Ceres	7 Iris	19 Fortuna	139 Juewa
2 Pallas	8 Flora	41 Daphne	144 Vibilia
4 Vesta	9 Metis	46 Hestia	356 Liguria
5 Astraea	12 Victoria	80 Sappho	554 Peraga
6 Hebe	16 Psyche	97 Klotho	694 Ekard

Near-Earth Asteroids

433 Eros	(Jurgens and Goldstein 1976, Campbell et al. 1976)
1566 Icarus	(Goldstein 1969, Pettengill et al. 1969).
1580 Betulia	(Pettengill et al. 1979)
1620 Geographos	(Ostro et al. 1985b)
1685 Toro	(Ostro et al. 1983, Goldstein et al. 1973)
1862 Apollo	(Ostro et al. 1985b, Goldstein et al. 1981)
1915 Quetzalcoatl	(Ostro et al. 1985b)
2100 Ra-Shalom	(Ostro et al. 1984, 1985b)
2101 Adonis	(Ostro et al. 1985b)
2201 Oljato	(Ostro et al. 1985b)

Comets

Encke	(Kamoun et al. 1982a)
Grigg-Skjellerup	(Kamoun 1983)
IRAS-Araki-Alcock	(Goldstein et al. 1984, Campbell et al. 1983)
Sugano-Saigusa-Fujikawa	(Campbell et al. 1983)

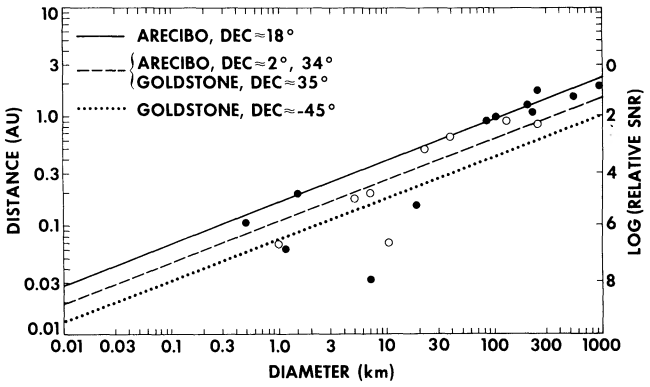

FIG. 1–Radar detectability of asteroids and comets for the Arecibo λ13-cm and Goldstone λ3.5-cm systems. The lines show the distance at which echoes from a target with a given diameter can be detected at a signal-to-rms-noise ratio (*SNR*) of 5. The calculations assume a radar albedo $\hat{\sigma} = 0.1$, a rotation period $P = 10$h, an equatorial view ($\delta = 0°$), and a single day's observation. The dependence of detection threshold on target declination follows from the sensitivity of each radar system to zenith angle. The filled circles correspond to about one-third of the radar-detected asteroids and comets. Empty circles represent several of the objects targeted for observations during the next few years.

II. Radar Techniques and Echo Detectability

The basic strategy in radar astronomy is to transmit a signal with known properties (intensity, polarization, time/frequency structure) for a duration similar to the round-trip propagation time to the target, receive the echo for a comparable duration, compare the properties of the echo to those of the transmission, and infer from this comparison the target's radar properties (e.g., radar cross section, echo spectral shape, and polarization ratio). The jump from radar properties to physical properties (e.g., dimensions, surface slope statistics, metal abundance) is in principle straightforward but in practice complex, and depends strongly on what we know a priori about the particular target, as will be demonstrated below.

How close to earth must an asteroid or comet be for its radar echo to be detectable? For a given transmitted power P_T and antenna gain G, the power flux a distance R from the radar will be $P_T G/4\pi R^2$. We define the target's radar cross section σ as 4π times the back-scattered power per steradian for unit incident flux at the target. We also define the antenna's effective aperture, $A_e \equiv G\lambda^2/4\pi$, with λ the radar wavelength. Then the total received power can be written:

$$P_R = P_T G^2 \lambda^2 \sigma/(4\pi)^3 R^4 \quad .$$

To be detectable, this power must exceed fluctuations in the background receiver noise by some comfortable margin. That noise can be shown to be chi-square distributed with $\nu = 2B\tau$ degrees of freedom, where B is frequency resolution and τ is integration time. For $\nu >> 10$, the distribution is nearly Gaussian with standard deviation $kT_sB/(B\tau)^{1/2}$, with k Boltzmann's constant and T_s the receiver system temperature. If the target has a diameter D and spin period P, we can write $B \sim D/P$ and $\hat{\sigma} \equiv \sigma/(\pi D^2/4)$, where $\hat{\sigma}$ is the radar albedo. Substituting, we have:

$$SNR \sim (P_T G^2/T_S)\, R^{-4}\, \hat{\sigma}\, D^{3/2} P^{1/2} \quad .$$

Adopting "typical" asteroid values of $\hat{\sigma} = 0.1$ and $P = 10$ h, we have *SNR* as a function of R and D for any given set of radar-system parameters. Figure 1 shows the detectability thresholds corresponding to the 5-standard-deviation level (which is quite safe for the sizes of the data sets of interest) for the λ13-cm system of the Arecibo Observatory and the λ3.5-cm system of the Goldstone Solar System Radar. Points are plotted for a few detected objects (filled circles) as well as for several potential future targets (open circles). The inverse-fourth-power dependence of *SNR* on distance severely limits the number of radar detectable asteroids and comets, and restricts observations to the closest approaches of targets to earth. For the Arecibo telescope, the narrow declination window (18°.3 ± 20°) is an additional limitation.

III. Target Characterization: Radar Properties and Physical Properties

All radar observations of comets and nearly all observations of asteroids have involved transmission of an unmodulated, highly monochromatic ("cw") waveform. Because the target is rotating, the echo is Doppler broadened into a power spectrum with a full bandwidth $B = (4\pi D/\lambda P)\cos\delta$, where P is the synodic spin period and δ is the acute angle between the radar line of sight $\boldsymbol{e}$ and the asteroid's spin vector $\boldsymbol{p}$. D is the sum of the two

distances, r_+ and r_-, measured from the plane containing $\boldsymbol{e}$ and $\boldsymbol{p}$ to those backscattering elements having the greatest positive (approaching) and negative (receding) line-of-sight velocities. For a sphere whose center of mass is also the center of figure, $D = 2r_+ = 2r_-$ is simply the diameter. For asteroids, which rarely are spherical and might be very irregular in shape and/or internal structure, r_+ and r_- can be different for any given rotational phase ϕ. (Of course, $r_+(\phi) \equiv r_-(\phi + \pi)$.) Perhaps the most lucid definition of D for a rigid target is: "D is the breadth, measured normal to $\boldsymbol{e}$, of the target's polar silhouette or, equivalently, of that silhouette's convex hull." Radar spectra obtained at several widely separated rotational phases provide a polygonal approximation to that convex hull if one knows P (from photoelectric light curves) and the Doppler shift for the target's center of mass (from a priori or a posteriori ephemerides). Estimation of the scale of the hull, i.e., of the silhouette's maximum breadth, D_{max}, requires knowledge of δ. Unfortunately, echo strength often limits one to just a lower bound on D_{max}. (Constraints on dimensions from delay-resolved echoes are potentially more powerful than those from cw observations, but they also place especially severe demands on the ephemeris, data-acquisition hardware and software, and data reduction.)

Integrating the echo power spectrum gives the target's radar cross section σ, and dividing σ by the target's projected area gives the radar albedo $\hat{\sigma}$, which is a useful measure of the target's intrinsic reflectivity, analogous to the geometric albedo employed in optical planetary astronomy. (A smooth metallic sphere would have a radar albedo of unity and a geometric albedo of 1/4.) Since the radar astronomer selects the transmitted and received polarizations, any albedo estimate must be identified accordingly. The most common approach in asteroid/comet observations has been to transmit a circularly polarized wave and to use separate receiving systems for simultaneous reception of the same sense of circular polarization as transmitted (i.e., the SC sense) and the opposite (OC) sense. The handedness of a circularly polarized wave is reversed on normal reflection from a smooth dielectric interface, so the OC sense dominates echoes from targets that look smooth at the radar wavelength. In this context, a surface with minimum radius of curvature very much larger than λ would "look smooth." Single scattering from rough surfaces, multiple scattering from smooth surfaces, or certain subsurface refraction effects can produce SC echo. The circular polarization ratio, μ_c, of SC to OC echo power is thus a useful measure of near-surface "roughness." Note that in contrast to the radar cross section and the echo bandwidth, both of which require accessory information about the target's spin vector and/or dimensions to constrain the target's physical properties, μ_c is an intensive radar property of the target. Moreover, estimation of μ_c is relatively uncorrupted by systematic (i.e., calibration or model-dependent) sources of error.

If μ_c is close to zero, its physical interpretation is unique, as the surface must be smooth at all scales within about an order of magnitude of λ and there can be no subsurface structure at those scales within several $1/e$ power absorption lengths, L, of the surface proper. In this special situation, we may interpret the radar albedo as the product gR (Pettengill 1978), where R is the Fresnel power-reflection coefficient at normal incidence and the backscatter gain g depends on target shape, the distribution of surface slopes with respect to that shape, and target orientation. Both R and L depend on very interesting characteristics of the surface material, including bulk density, porosity, particle-size distribution, and metal abundance. Clearly, our ability to exploit fully a target's radar signature rests on what we know about a target's dimensions and about its orientation during the radar observations. Since estimation of g is tantamount to determination of the target's back-scattering law from the bandwidth and functional form of the echo spectrum, prior knowledge of the direction and magnitude of the spin vector is critical.

Inference of physical properties from radar properties is therefore an iterative, bootstrapping procedure whose success is optimized by acquisition of high-quality photoelectric light curves and stellar-occultation timing data for viewing geometries similar to those during the radar observations. This situation has been most closely realized for the large (538-km-diameter) main-belt asteroid 2 Pallas.

IV. Pallas: A Case Study of the Best Characterized Asteroid

A. *Small-Scale Structure*

Figure 2 shows OC and SC echo-power spectra obtained by Ostro, Campbell, and Shapiro (1985*a*) at λ13 cm for Pallas. Their estimate of Pallas's circular polarization ratio, 0.05 ± 0.02, is smaller than values of μ_c estimated with similar precision at decimeter wavelengths for any other planetary object except perhaps for Venus, for which values between 0.04 and 0.06 have been reported. Thus, Pallas is one of the smoothest objects in the solar system at decimeter scales.

Asteroids as large as 100 km are expected to be blanketed by extremely thick regoliths (Housen and Wilkening 1982), and Pallas's very low μ_c reveals its upper regolith to be very smooth, soft, and fine-grained, containing few particulates as large as a centimeter. Pallas's VIS/IR reflection spectrum resembles those of C1–C2 carbonaceous chondrites (Larson et al. 1979), and the smoothness of Pallas's surface might be due to the relative weakness and susceptibility to comminution of those meteorites, which are lacking in free metal and

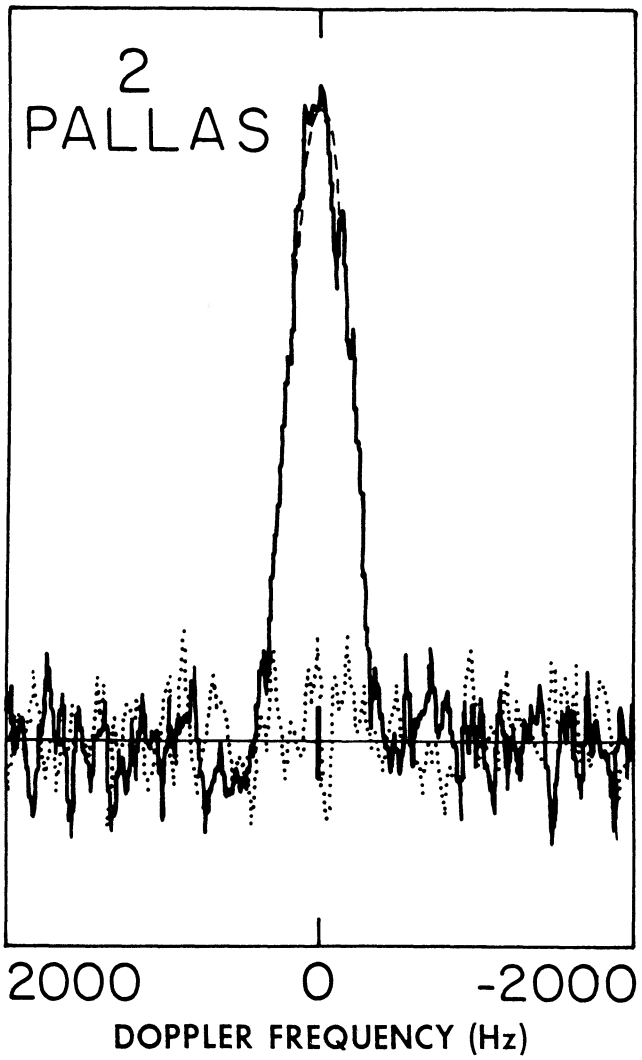

FIG. 2–Radar-echo-power spectra obtained for asteroid 2 Pallas, smoothed to a frequency resolution of 40 Hz. Echo power (arbitrary linear scale) is plotted against Doppler frequency (Hz). The circular polarization ratio, μ_c, of power received in the same sense of circular polarization as transmitted (i.e., the SC sense; dotted curve) to that in the opposite, or OC sense (solid curve) is 0.05 ± 0.02, indicating an extremely smooth surface at decimeter scales. However, the model (dashed curve) fit to the OC spectrum indicates that the surface is very rough compared to, say, the moon at some scale(s) no smaller than several meters and possibly as large as many kilometers. (See text.) Based on Figure 1 of Ostro et al. (1985*a*).

enriched in volatiles compared to ordinary chondrites or differentiated meteorites.

B. *Large-Scale Structure*

Additional information about Pallas's surface follows from analysis of the OC echo spectrum, via estimation of $B = (4\pi D/\lambda P)\cos\delta$, $\hat{\sigma}$, g, and $R = \hat{\sigma}/g$. Two separate stellar occultations have constrained this asteroid's dimensions exceptionally well (Wasserman et al. 1979; Dunham et al. 1983; Chapman 1984). Pallas's figure is nearly spherical, with a mean diameter of about 538 km and a maximum equatorial axis of about 559 km. From light curves (e.g., Binzel 1984), we know the rotation period ($P = 7^h.811$) and find that the rotational phases covered by the radar observations included the orientation placing the maximum breadth, $D_{max} = 559$ km, normal to the line of sight. Thus we can write $B = (4\pi D_{max}/\lambda P)\cos\delta = 1980\cos\delta$. Since the half-power bandwidth B_{HP} is about 500 Hz, we know that $B_{HP}/B \approx 500/(1980\cos\delta) \geq 0.25$. In contrast, lunar echo spectra are much more sharply peaked ($B_{HP}/B \leq 0.1$), so the moon is much more limb-darkened than Pallas, and Pallas must be much rougher than the moon at some scale(s) no smaller than several meters.

A commonly used gauge of large-scale roughness is the rms surface slope, s_0. Models of lunar spectra yield $s_0 \approx 6°$, so Pallas's value must be much larger. If we knew Pallas's pole direction and hence δ and B, we could estimate s_0 quite accurately. Lacking such information, Ostro et al. (1985*a*) estimated s_0 and B simultaneously by fitting to the echo spectrum a model derived for a sphere whose back-scattering law assumes that the surface height distribution and lateral autocorrelation function are Gaussians. Their least-squares solution yielded a model (barely visible as the dashed curve in Fig. 2) with low postfit residuals and parameter estimates: $B = 1100 \pm 80$ Hz and $s_0 = 27° \pm 3°$. These parameters are very highly correlated ($ds_0/d\delta \approx$ one degree of rms slope per degree of declination), but the fine agreement between their declination estimate (56° ± 3°) and Binzel's (1984) constraints on Pallas's pole direction derived from optical light curves lends confidence to the validity of the radar results (Fig. 3).

Deviation of Pallas's figure from a sphere may have introduced some positive bias into the estimation of s_0, but it is difficult to assess the magnitude of that bias. My guess is that the "true" bias-corrected value of Pallas's rms slope is within 5° of 20°. This inference seems reasonable given that the maximum stable slope of a fine-grained regolith (i.e., its angle of repose) can be expected to lie in the 30°–35° range (Stiegler 1976). Very much larger slopes, say ≈ 45°, cannot be common or they would be expected to give rise to multiple scattering and depolarization, which is not observed.

The preceding discussion suggests that Pallas's surface is "morphologically smooth but topographically rough." We cannot determine the scale(s) of the topography (i.e., of the large-rms-slope component). However, preliminary results from Pallas's occultation of 1 Vulpeculae presented by Chapman (1984) indicate that the surface might be extremely rough at scales of many kilometers.

C. *Regolith Bulk Density and Porosity*

Combining estimates for Pallas's radar cross section, projected area, and rms surface slope, Ostro et al. (1985*a*) obtain $\hat{\sigma} = 0.092 \pm 0.024$ and $g \simeq 1.1$, so $R \approx 0.08 \pm 0.02$.

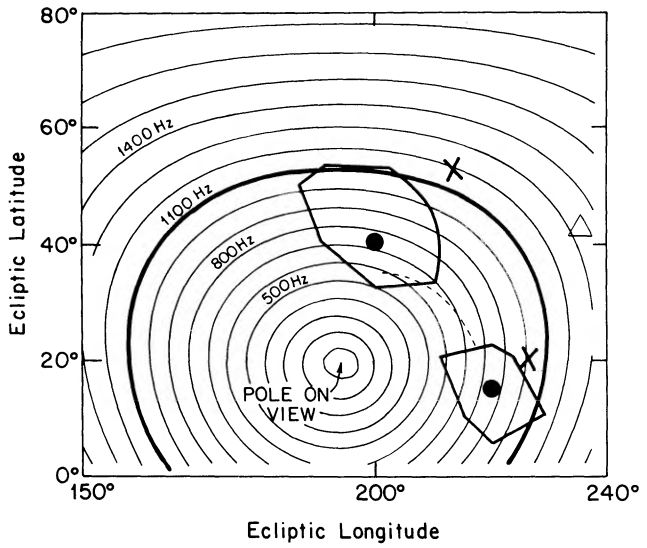

FIG. 3–Constraints on the pole direction of asteroid 2 Pallas. Radar echoes obtained for Pallas in March 1982 have a bandwidth $B = 1980 \cos\delta$, where δ is the asteroid-centered declination of earth. (See text.) The concentric contours are loci of Pallas pole directions corresponding to constant B and δ. For instance, if the pole direction were parallel to Pallas's geocentric direction (ecliptic long = 195°, lat = 19°) during the observations, the radar would have had a pole-on view ($\delta = 90°$, $B = 0$ Hz). However, the echo spectrum in Figure 2 has a bandwidth larger than 500 Hz (and hence excludes pole directions inside the 500-Hz contour) at a high confidence level. The model (dashed curve in Fig. 2) fit to the data yields $B = 1100 \pm 80$ Hz. The large dots and polygons are pole-direction estimates and error fields obtained by Binzel (1984) from analyses of optical light curves. The crosses were obtained by J. Lambert (Binzel 1984) from a different light-curve analysis technique. The next Pallas radar opportunity, in 1987, can provide a second set of such contours, but centered on the triangle. In 1996, Pallas will be detectable at high *SNR* all along the dashed curve.

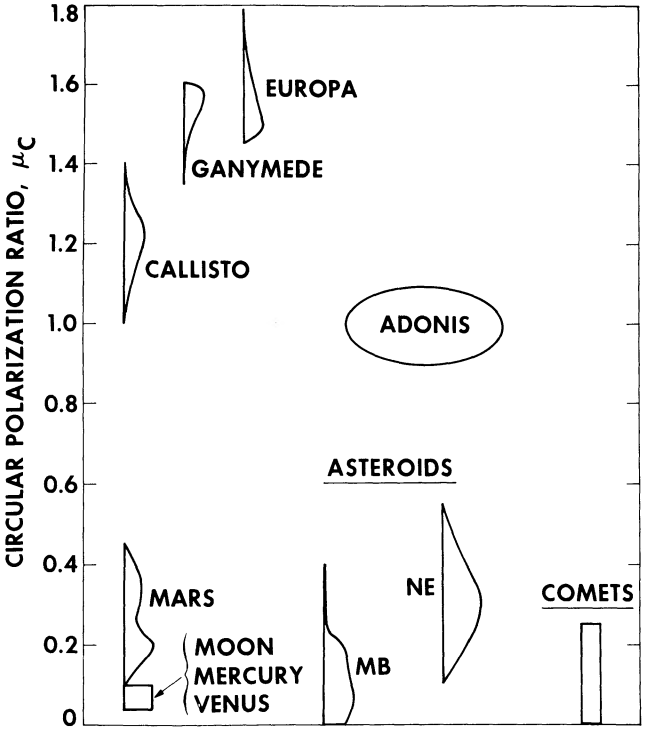

FIG. 4–Circular polarization ratios of radar-detected planetary targets (see text and Fig. 2). Approximate distributions of available estimates of μ_c are sketched for the icy Galilean satellites (Ostro et al. 1980), Mars (Harmon and Ostro 1985), main-belt asteroids (Ostro et al. 1985*a*), and near-earth asteroids (Ostro et al. 1985*b*). The curve for near-earth asteroids excludes 2101 Adonis, whose polarization ratio, 1.0 ± 0.2, is close to values obtained for Callisto.

Laboratory measurements of the electrical properties of rock powders by these authors (see also Olhoeft 1979) indicate that if the regolith is vertically homogeneous, then the estimate for R corresponds to a density, $d = 1.8 \pm 0.2$, and $L \approx$ several meters. If the specific gravity of Pallas's surface material is within the range (2.2–2.9; Buchwald 1975) of C1 and C2 carbonaceous chondrites, then the hypothetical regolith porosity would be between 0.1 and 0.5. This interval overlaps the range (0.3 to 0.7) of estimates of the porosity of lunar soil (Carrier, Mitchell, and Mahmood 1973).

V. Main-Belt Asteroid Surface Properties

A. *Surface Structure*

Occultation chords as abundant as those for Pallas are lacking for other radar-detected main-belt asteroids. Still, given the available constraints on these object's spin vectors, dimensions, and hence maximum echo bandwidths, Ostro et al. (1985*a*) claim that $B_{HP}/B > 0.2$ for main-belt asteroid spectra. These objects thus appear rougher than the moon at some scale(s) which, in light of their low polarization ratios (mean $\mu_c = 0.12$; rms dispersion = 0.10), probably exceed a few meters. The large-scale topography inferred for Pallas might well be a common characteristic of most large asteroids. Indeed, occultation evidence for a rough limb is also seen for Minerva (Millis et al. 1985) and possibly for Ceres (Hubbard et al. 1985). If large-scale topographic roughness is ubiquitous on large asteroids, its origin might involve the impact cratering process, whose manifestations are likely to be different on low-gravity, low-radius-of-curvature objects from those on the terrestrial planets (Cintala, Head and Veverka 1978).

Significant differences in the decimeter-scale surface morphologies of these objects is evident from the diversity of main-belt asteroid polarization ratios (Fig. 4). The precision of the ratio measurements preclude very strong statements about possible correlations with taxonomic type, but the available data suggest that the distributions of μ_c for S types and C types overlap each other, with the S types' distribution having the higher mean.

The largest circular polarization ratio estimated by Ostro et al. (1985*a*) is 0.40 ± 0.11 for 4 Vesta. This value is not very precise, but it still seems higher than the main-belt average at the several-standard-deviation level. Vesta's surface appears to have a basaltic composition, presumably the outcome of magmatic differentiation (Drake 1979). The apparently substantial degree of small-scale roughness on this object could be due to the rela-

tively high strength of basaltic rock; or, it might be evidence for an unusually young surface.

B. *Metal Abundance*

One of the simplifying assumptions in the Pallas analysis was the absence of free metal in the regolith. This assumption is invalid for S-type and M-type asteroids, which comprise about half of the main-belt radar sample. For these objects, knowledge of metal abundance would help to clarify meteoritic associations, and hence the extent to which these asteroids underwent postaccretion heating and chemical differentiation.

There is much disagreement surrounding inference of metal weight fraction (w) from VIS/IR reflection spectra (Gaffey 1984; Feierberg, Larson, and Chapman 1982). For radar observations, the reflectivities (R) derived from asteroid echoes can be combined with laboratory estimates of R for particulate mixtures of rock and metal to yield a joint constraint on w and porosity, p (Ostro et al. 1985*a*). The distribution of radar albedos ($\hat{\sigma}$) reported by those authors for 20 main-belt asteroids is extremely broad and implies large variations in porosity and/or metal concentration.

Consider the case of asteroid 16 Psyche, whose radar albedo (0.29 ± 0.11) is the highest estimated for a main-belt asteroid. The VIS/IR data suggest an association of Psyche's surface mineralogy with either enstatite chondrites ($w \leq 0.3$) or iron meteorites ($w > 0.9$). To satisfy Psyche's radar albedo, the first possibility would require a nearly solid surface, whereas the latter is compatible with porosities typical of lunar soil. The case is not closed, but the radar results favor the hypothesis that Psyche is a nearly entirely metallic asteroid, presumably the collisionally stripped core of a differentiated object.

For S types, the radar results provide a novel coupling between w and p, but the metal abundances for the candidate meteorite analogs, $w \approx 0.5$ for stony irons and $w < 0.2$ for ordinary chondrites, are insufficiently separated for one to choose reliably between the competing hypotheses.

VI. Near-Earth Asteroids

In analyzing results of radar, stellar occultation, and other ground-based data on the largest objects in the main belt, one usually can justify the assumption of a simple shape, at least as a first approximation. For small, near-earth asteroids and comets, that assumption stands on more tenuous theoretical ground, and a prime contribution of radar studies is to provide concrete dimensional constraints.

Jurgens and Goldstein (1976) pioneered this effort, applying techniques developed by Jurgens (1982) to model the λ3.5-cm radar signature of 433 Eros as due to echoes from a homogeneously scattering ellipsoid. They concluded that Eros's figure might be more egg-shaped than ellipsoidal. Ostro, Campbell, and Shapiro (1983) applied the same techniques to λ13-cm echoes from 1685 Toro and noted that the postfit residuals indicate significant departures from the simplified model, possibly including a surface feature with enhanced radar brightness and depolarization. (Incidentally, both these studies relied on estimates of δ from optical studies.) More recently, Ostro et al. (1984) reported radar and photoelectric observations of 2100 Ra-Shalom and combined their results with an IR radiometric estimate of this asteroid's projected area to constrain its linear dimensions, pole direction, and spin period. Again, the data seemed difficult to reconcile with a homogeneous, axisymmetric model.

For Toro (Fig. 5), 1862 Apollo, 1620 Geographos, and 2201 Oljato, pronounced variations in bandwidth as a function of rotational phase clearly reveal very noncircular polar silhouettes (Ostro, Campbell, and Shapiro 1985*b*). For Oljato, observed on four dates in July 1983, the spectra are bifurcated on one date but not on the other three. Possible explanations range from a highly irregular (grotesque?) shape to a regular shape with a bizarre albedo distribution.

As illustrated in Figure 4, the circular polarization ratios of near-earth asteroids tend to be larger than those of main-belt asteroids, indicating a greater degree of centimeter-to-meter-scale roughness on the smaller objects. This result is consistent with theoretical expectations of thin, rocky regoliths on small asteroids (Housen and Wilkening 1982). For several of the smaller objects observed at very high signal-to-noise levels, variations in μ_c

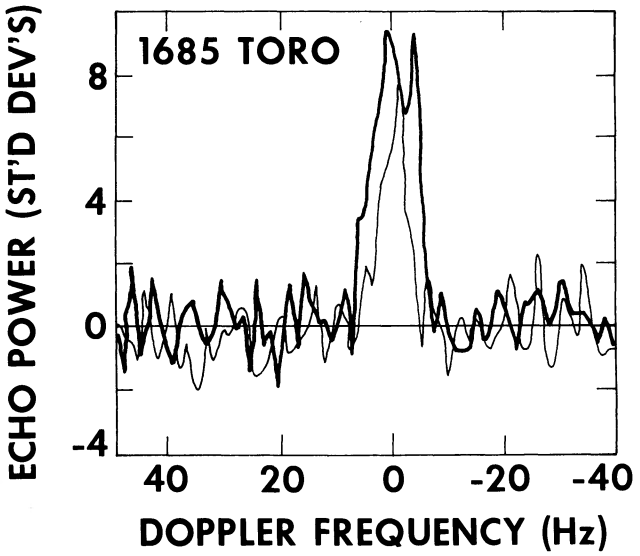

FIG. 5–Echo power spectra of asteroid 1685 Toro. Each curve has a frequency resolution of 1.2 Hz and is a weighted mean of OC data obtained at rotation phases within ~ 20° of "broadside" (heavy curve) or "end-on" (faint curve) views of the asteroid. Analyses of the complete radar data set (Ostro et al. 1983; Ostro and Connelly 1984) indicate that Toro's polar silhouette has breadth extrema in a ratio near 2.

with rotational phase are apparent, indicating heterogeneity at decimeter scales.

VII. The Unusual Asteroid 2101 Adonis

As Figure 4 demonstrates, the polarization ratio of 2201 Adonis is the highest obtained for any asteroid and is exceeded only by values obtained for Jupiter's icy Galilean satellites Europa, Ganymede, and Callisto (Ostro et al. 1980). The high abundance of water ice on those satellites is related to their unusual radar behavior but is not a sufficient condition, as evidenced by the fact that the available values of μ_c for (presumably ice-rich) comets are much less than unity. (For comet *IRAS*-Araki-Alcock, Goldstein et al. (1984) report $\mu_c \approx 0.25$. For comet Grigg-Skjellurup, from data described by Kamoun (1983), I calculate $\mu_c = 0.0 \pm 0.1$.) Perhaps the most likely explanation for the icy satellites' anomalous ratios is "refraction scattering" (Hagfors, Gold, and Ierkic 1985) from within a regolith containing symmetrical patterns of variations in refractive index. However, the detailed nature of the subsurface structure responsible for the icy Galilean satellites' polarization ratios is not yet clear.

I believe that a possible key to understanding the radar behavior of these objects and Adonis involves the low-temperature sublimation of ice out of a solid dispersion of clay particles in water ice, as described by Saunders et al. (1985). Their laboratory-produced residues reach densities of 0.001 g cm^{-3}, suggesting that one might expect several orders of magnitude of density variation (and hence refractive-index variation) on a planetary surface where such residues comprise much of the regolith. Formation of symmetrical patterns of density variation, such as the "fish eyes" of Hagfors et al., might arise from subsurface sublimation of volatiles, or might be catalyzed by meteoritic impacts within a certain energy regime. As noted by Drummond (1982), Adonis's orbital association with meteor streams suggests that this asteroid might be an extinct cometary nucleus. Adonis's μ_c is certainly not "cometary" (see Fig. 4) and VIS/IR observations of Adonis reveal no cometary activity. However, the same statements hold for Europa, Ganymede, and Callisto.

The icy Galilean satellites also have huge radar albedoes, ranging from about 0.3 for Callisto to about unity for Europa. For Adonis, there are estimates of visual magnitude and radar cross section, but no color indices or IR radiometric results have been reported and tight constraints on Adonis's size or (visual or radar) albedo are unavailable. Nonetheless, I find that the existing data are compatible with Adonis having albedoes comparable to Callisto's, in which case Adonis's "areal diameter" would be about half a kilometer. Estimates of μ_c for Callisto have a weighted mean of 1.2 ± 0.1, but a large fraction of the trailing (optically brighter) hemisphere seems to have $\mu_c \approx 1.0$ (Ostro 1982).

The hard information is sparse, but it seems clear from the radar results that Adonis is very different from other asteroids and (active) comets. Given the dynamical arguments and the apparent similarity between the radar properties of Adonis and Callisto, we should consider the notion that Adonis might be an extinct cometary nucleus.

VIII. Comets

Only four comets have been detected by radar (Table I), but prospects are high for detecting Halley if its diameter is as large 20 km, as suggested by Cruikshank, Hartmann, and Tholen (1985). Otherwise, the next promising comet opportunity is in late 1987, with Denning-Fujikawa.

Radar is much more capable of unambiguous detection of a cometary nucleus than VIS/IR methods, but the difficulties encountered in interpreting the radar properties of an asteroid for which we lack reliable independent constraints on spin vector and dimensions are exacerbated for a comet (Kamoun, Pettengill, and Shapiro 1982*b*). Even so, the radar data provide useful interval estimates on nuclear dimensions, and the radar signature of one particular comet (*IRAS*-Araki-Alcock) revolutionizes our concepts of the physical nature of these intriguing entities.

Comet *IRAS*-Araki-Alcock came within 0.03 AU of earth in May 1983, permitting acquisition of echoes at Goldstone (Goldstein et al. 1984) and Arecibo (Campbell et al. 1983) with higher signal-to-noise ratios than those obtained to date for any other comet or asteroid. The echoes have a narrow-band component from the nucleus as well as a much weaker broad-band component (Fig. 6). The latter arises from scatterers whose line-of-sight velocity distribution indicates that most are not gravitationally bound to the nucleus. Goldstein et al. (1984) argue that most of the particles, which must be at least a centimeter in size, escaped from the ~ 7-km-diameter nucleus to form a debris swarm whose size is $\geq 10^4$ km. Echo spectra for the nucleus indicate a nonspherical shape and show several features that are consistent with roughness on meter-to-km scales. Thus, one envisions this object as extremely rough, with an explosively active surface from which chunks of solid material are being blasted into space by subsurface sublimation of volatiles.

IX. Summary

The last few years of radar observations provide our first information about the nature of these objects at centimeter-to-kilometer scales. There is tremendous diversity in the decimeter-scale characteristics of asteroids and comets. The surfaces of many, if not most, large asteroids appear much rougher than the moon at some scale(s) between several meters and many kilometers. The radar albedoes of the 20 radar-detected main-belt asteroids support inferences from VIS/IR reflectance spectroscopy that these objects' surface concentrations of

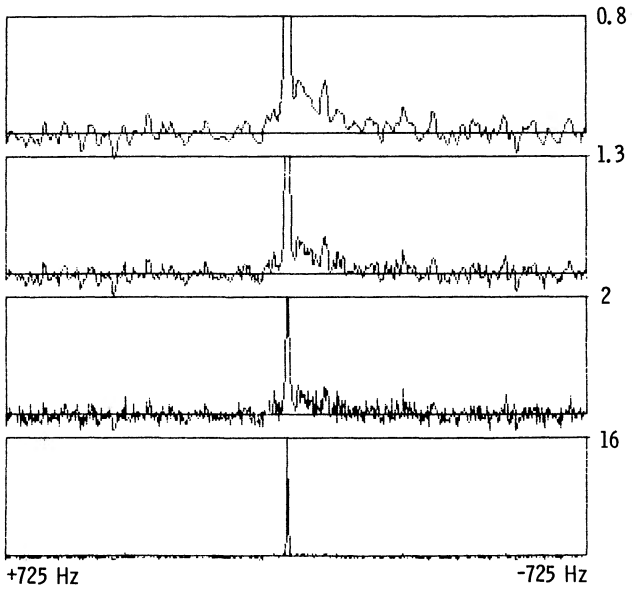

FIG. 6–Echo power spectrum of comet *IRAS*-Araki-Alcock obtained by Goldstein et al. (1984), shown here with four different vertical truncations and degrees of smoothing. Echo power is plotted against Doppler frequency. The narrow spike is echo from the comet's ~ 7-km nucleus. The broad-band component, or "skirt," is echo from a $\geq 10^4$- km debris swarm consisting of particles no smaller than a centimeter and, for the most part, not gravitationally bound to the nucleus.

metal range from ~ 0.0 to ~ 1.0, presumably arising from great variations in these objects' initial compositions and thermal histories.

For the smaller, near-earth asteroids, the recent radar data furnish direct evidence for nonspherical and occasionally very irregular shapes, as well as for very heterogeneous surfaces. The proliferation of striking, peculiar echoes among such a small sample suggests that this is a very exotic population indeed. Given the fascinating echo spectra of *IRAS*-Araki-Alcock, that conclusion is probably equally valid for comets.

Observations planned for the remainder of this decade can more than double the current number of radar-detected asteroids and comets and should clarify the distributions of these objects' radar properties. As demonstrated herein, the scientific value of radar data for any given target depends in large measure on the availability of VIS/IR results, especially occultation chords and photoelectric light curves. On a more fundamental level, the physical ramifications of the growing collection of ground-based data on asteroids and comets will not be fully appreciated until we have reliable fiducials to calibrate our interpretations of those data. The Halley and Amphitrite flybys are the first steps in this direction, and will inaugurate a new era in asteroid and comet astronomy.

I thank K. Banwart for secretarial assistance. This research was conducted at the Jet Propulsion Laboratory, California Institute of Technology, under contract with the National Aeronautics and Space Administration.

REFERENCES

Binzel, R. P. 1984, *Icarus* **59**, 456.
Buchwald, V. F. 1975, *Handbook of Iron Meteorites* (Berkeley: University of California Press), p. 62.
Campbell, D. B., Pettengill, G. H., and Shapiro, I. I. 1976, *Icarus* **28**, 17.
Campbell, D. B. et al. 1983, *Bull. A. A. S.* **15**, 800.
Carrier III, W. D., Mitchell, J. K., and Mahmood A., 1973, *Proc. Fourth Lunar Sci. Conf.* (New York: Pergamon).
Chapman, C. R. 1984, *Planetary Report 4* Jul/Aug, 12.
Cintala, M. J., Head, J. W., and Veverka, J. 1978, *Proc. Lunar Planet Sci. Conf.* **9**, 3803.
Cruikshank, D. P., Hartmann, W. K., and Tholen, D. J. 1985, *Nature* **315**, 122.
Drake, M. J. 1979, in *Asteroids*, T. Gehrels, ed. (Tucson: University of Arizona), p. 765.
Drummond, J. D. 1982, *Icarus* **49**, 143.
Dunham, D. W. et al. 1983, *Bull A. A. S.* **15**, 822.
Feierberg, M. A., Larson, H. P., and Chapman, C. R. 1982, *Ap. J.* **257**, 361.
Gaffey, M. J. 1984, *Icarus* **60**, 83.
Goldstein, R. M. 1969, *Icarus* **10**, 430.
Goldstein, R. M., Holdridge, D. B., and Lieske, J. H. 1973, *A.J.* **78**, 508.
Goldstein, R. M., Jurgens, R. F., and Yeomans, D. K. 1981, *Icarus* **48**, 59.
Goldstein, R. M., Jurgens, R. F., and Sekanina, Z. 1984, *A.J.* **89**, 1745.
Hagfors, T., Gold, T., and Ierkic, H. M. 1985, *Nature* **315**, 637.
Harmon, J. K., and Ostro, S. J. 1985, *Icarus* **62**, 110.
Housen, K. R., and Wilkening, L. L. 1982, *Ann. Rev. Earth Planetary Sci.* **10**, 355.
Hubbard, W. B. et al. 1985, *Lunar Planet. Sci. Conf. 16 Abstracts*, 370.
Jurgens, R. F. 1982, *Icarus* **49**, 97.
Jurgens, R. F., and Goldstein, R. M. 1976, *Icarus* **28**, 1.
Kamoun, P. G. D. 1983, Ph.D. Thesis, Massachusetts Institute of Technology.
Kamoun, P. G., Campbell, D. B., Ostro, S. J., Pettengill, G. H., and Shapiro, I. I. 1982*a*, *Science* **216**, 293.
Kamoun, P. G., Pettengill, G. H., and Shapiro, I. I. 1982*b*, in *Comets*, L. L. Wilkening, ed. (Tucson: University of Arizona), p. 288.
Larson, H. P., Feierberg, M. A., Fink, U., and Smith, H. A. 1979, *Icarus* **39**, 257.
Millis, R. L. et al. 1985, *Icarus* **61**, 124.
Olhoeft, G. R. 1979, *U.S. Geological Survey Open File Report* 79-993.
Ostro, S. J. 1982, in *Satellites of Jupiter*, D. Morrison, ed. (Tucson: University Arizona Press), p. 213.
Ostro, S. J., and Connelly, R. 1984, *Icarus* **57**, 443.
Ostro, S. J., Campbell, D. B., Pettengill, G. H., and Shapiro, I. I. 1980, *Icarus* **44**, 431.
Ostro, S. J., Campbell, D. B., and Shapiro, I. I. 1983, *A.J.* **88**, 565.
Ostro, S. J., Harris, A. W., Campbell, D. B., Shapiro, I. I., and Young, J. W. 1984, *Icarus* **60**, 391.
Ostro, S. J., Campbell, D. B., and Shapiro, I. I. 1985*a*, *Science* **229**, 442.
Ostro, S. J. Campbell, D. B., and Shapiro, I. I. 1985*b*, *Bull A.A.S.* **17**, 729.
Pettengill, G. H. 1978, *Ann. Rev. Astr.* **16**, 265.
Pettengill, G. H. et al. 1969, *Icarus* **10**, 432.
Pettengill, G. H., Ostro, S. J., Shapiro, I. I., Marsden, B. G., and Campbell, D. B. 1979, *Icarus* **40**, 350.
Saunders, R. S., Parkes, T. J., Stephens, J. B., Lane, E. G., and Fanale, F. P. 1985, *Lunar Planet. Sci. Conf. 16 Abstracts*, 730.
Stiegler, S. E. 1976, *A Dictionary of Earth Sciences.* (New York: Pica Press), p. 14.
Wasserman, L. H. et al. 1979, *A.J.* **84**, 259.